



Methanol dehydration to dimethylether over Al_2O_3 catalysts

Siranush S. Akarmazyan^a, Paraskevi Panagiotopoulou^a, Anastasios Kambolis^b, Christina Papadopoulou^b, Dimitris I. Kondarides^{a,*}

^a Department of Chemical Engineering, University of Patras, GR-26504 Patras, Greece

^b Department of Chemistry, University of Patras, GR-26504 Patras, Greece

ARTICLE INFO

Article history:

Received 15 October 2012

Received in revised form

21 November 2012

Accepted 27 November 2012

Available online 5 December 2012

Keywords:

Dimethyl ether

Methanol

Al_2O_3

TPD

DRIFTS

Transient-MS

ABSTRACT

The vapor-phase dehydration of methanol to dimethylether (DME) has been investigated over a set of eight commercial and self-prepared Al_2O_3 catalysts with different physicochemical characteristics. Materials were characterized with respect to their textural properties (B.E.T. and B.J.H. methods), acidity (TPD of ammonia), crystallinity, phase composition and morphology (XRD, TEM). Catalytic activity and selectivity have been evaluated in the temperature range of 150–400 °C in the absence and in the presence of water in the feed. The adsorption/desorption properties of catalysts toward methanol and water as well as some aspects of the reaction mechanism have been investigated with the use of transient-MS and *in situ* DRIFTS techniques. Results show that catalytic activity per gram of catalyst varies by two orders of magnitude from one sample to another in a manner that depends on the physicochemical characteristics of Al_2O_3 . All samples investigated are highly selective to DME at temperature lower than ca. 325 °C, whereas small amounts of CO and CH_4 are formed at higher reaction temperatures. As a general trend, activity per gram of catalyst increases with increase of SSA (amount of acidic surface sites) and is enhanced over samples characterized by high crystallinity and relatively high porosity. The presence of water vapor in the feed suppresses conversion of methanol at a given temperature due to competition for active sites and thermodynamic limitations. Methanol adsorbs on the Al_2O_3 surface both molecularly and in the form of methoxy species. Evidence is provided that formation of DME involves weakly adsorbed methoxy species whereas methoxy species that are bonded more strongly on the Al_2O_3 surface are converted to surface formates, which decompose to yield CO, H_2 and CH_4 in the gas-phase.

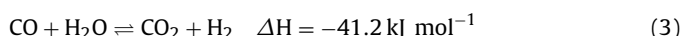
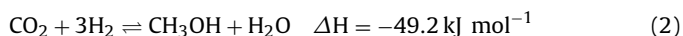
© 2012 Elsevier B.V. All rights reserved.

1. Introduction

Dimethyl ether (CH_3OCH_3 , DME) is a non-toxic liquefied gas, which is projected to become one of the fundamental chemical feedstocks in the 21st century [1,2]. Among others, DME can be used as a propellant in aerosol formulations [3,4], as a precursor for the synthesis of other organic compounds, such as dimethyl sulphate, methyl acetate, ethylidene diacetate and light olefins [5–8], as an alternative, clean and environmentally benign fuel for compression-ignition engines [9–12] and gas turbines [13], and as a source of hydrogen for fuel cell applications [5,14–17]. Moreover, DME may serve as an efficient hydrogen carrier [2], which could be used to store renewable energy in a chemical form that is easy to handle, distribute, store and use. In particular, hydrogen produced from excess electricity of wind turbines or photovoltaics *via* water electrolysis could be used to hydrogenate carbon dioxide into

methanol/DME thereby providing a means of recycling CO_2 into useful chemicals, with obvious environmental benefits [18–20].

Dimethylether can be produced from synthesis gas ($\text{CO}/\text{H}_2/\text{CO}_2$) originating from natural gas, coal or biomass *via* a two-step process that involves synthesis of methanol by hydrogenation of CO/CO_2 over a copper based catalyst (e.g., $\text{CuO-ZnO-Al}_2\text{O}_3$) and subsequent dehydration of methanol to DME over an acidic catalyst (e.g., $\gamma\text{-Al}_2\text{O}_3$ or ZSM5) [10,19,21,22]:



Alternatively, DME can be produced from synthesis gas in a one-step (direct) process using a hybrid (bifunctional) catalyst system that permits both methanol synthesis and dehydration in a single process unit [23–25]. Thermodynamic limitations imply that methanol synthesis from CO (1) or CO_2 (2) is favored at low temperatures and high pressures [26,27]. These constraints can be reduced by co-production of DME because the equilibrium constant

* Corresponding author. Fax: +30 2610 991527.

E-mail address: dimi@chemeng.upatras.gr (D.I. Kondarides).

of the methanol dehydration reaction is much higher than that of methanol synthesis [18]. Water formed by methanol dehydration (4) can be removed from the system by the water gas shift (WGS) reaction (3), which also results in a shift of the equilibrium composition toward the desired direction [28,29].

The rate of the methanol dehydration reaction (4) depends strongly on the acidity of catalyst employed. In this respect, several solid acid catalysts have been investigated including Al_2O_3 [21,30–33], zeolites [22,30,34–37] and mixed metal oxides [12,30,31,34,35,38–41]. Among these, the most extensively studied materials are based on Al_2O_3 . This is because Al_2O_3 is characterized by high surface area, excellent thermal stability, high mechanical resistance and suitable acidity for the reaction that yields good performance in terms of methanol conversion and DME selectivity, the latter being almost 100% [21,33,37–39,41]. A disadvantage of Al_2O_3 is that, due to its hydrophilic nature, it has the tendency to adsorb by-product water more strongly than methanol and, therefore, loses part of its activity during the reaction [30,41,42]. Thus, it is important to develop active, selective and stable methanol dehydration catalysts characterized by high resistance to water produced by CO/CO_2 hydrogenation reactions (1) and (2).

A detailed investigation is being carried out in the present laboratories in an attempt to identify the key parameters that determine the catalytic activity of solid acids, including Al_2O_3 , modified Al_2O_3 and zeolites, for the dehydration of methanol to DME. The aim is to develop an efficient, selective and stable catalyst that could be then combined with a methanol synthesis catalyst and used for the direct conversion of syngas and/or CO_2/H_2 mixtures into methanol/DME. In the present study, dehydration of methanol to DME is investigated over a number of commercial and self-prepared Al_2O_3 catalysts with emphasis given on the effects of physicochemical characteristics of materials on catalytic performance and on the elucidation of the reaction mechanism in the presence and in the absence of water in the feed.

2. Experimental

2.1. Catalyst preparation and characterization

A variety of commercial and self-prepared Al_2O_3 catalysts in powder form were used to study the effects of physicochemical characteristics on catalytic performance for the title reaction. Commercial catalysts investigated (see Table 1 for suppliers and notations) include an α - Al_2O_3 sample (denoted as Al1) and five different γ - Al_2O_3 samples (Al2 to Al6). All materials were used as received, with the exception of Al6 (AKZO), which was first treated as described in "Supplementary information".

Self-prepared Al_2O_3 samples were synthesized employing two different sol-gel methods (SG1, SG2). The SG1 catalyst was synthesized following a preparation procedure similar to that described by Keshavarz et al. [43]. Aluminum isopropoxide $\text{Al}(\text{OC}_3\text{H}_7)_3$

(Fluka, purum >97%) and hexadecyl-trimethyl-ammonium bromide $\text{C}_{19}\text{H}_{42}\text{BrN}$ (Merck, for synthesis), denoted as Aliso and CTAB respectively, were dissolved in an appropriate amount of isopropanol. The molar ratio CTAB/(Aliso) was 0.8. The hydrolysis step was carried out at 70 °C by a dropwise addition of a water-isopropanol solution ($\text{H}_2\text{O}/\text{Aliso}$ molar ratio = 90) under vigorous stirring. The mixture was peptized under stirring by adjustment of the pH to 5.5, using HNO_3 (10 wt%). Afterwards it was left to age at ambient temperature for 2 h. The sample was finally dried at 110 °C overnight and calcined at 450 °C for 5 h and then at 600 °C for 30 min for the complete removal of the organic precursor. For the synthesis of the SG2 catalyst, an aqueous solution of ethanol was first prepared and its pH was adjusted at 2 with the use of HNO_3 . The mixture was then added into an ethanol solution of $\text{Al}(\text{OC}_3\text{H}_7)_3$ (Alfa Products) under vigorous stirring and a gel was formed. The gel was left at 25 °C under stirring for 24 hours until nearly all the liquid was evaporated. The solid residue was dried at 120 °C for 12 h, calcined in air at 600 °C for 3 h and stored in a sealed vial. Sample powders were pelletized without binder in a hydraulic press and then crashed and sieved to the required mesh size (0.18 < d < 0.25 mm).

Materials were characterized with respect to their textural properties (specific surface area (SSA) and the porosity) using a Micromeritics TriStar 3000 equipment. Moisture and other substances, adsorbed on the surface of the samples, were removed *in situ* by heating at 573 K for 1 h under a stream of nitrogen. SSAs were calculated following the standard B.E.T. equation for nitrogen relative pressure range $0.06 < P/P_0 < 0.20$. Pore size distribution of the samples was determined following the Barret–Joyner–Halenda (BJH) method at liquid nitrogen temperature (−196 °C) using the apparatus software. X-ray diffraction (XRD) analysis was performed using a Bruker D8 Advance diffractometer equipped with a Ni-filtered Cu radiation ($K_{\alpha 1} = 0.15418 \text{ nm}$) and a LynxEye detector, operated at 40 kV and 40 mA. The diffraction patterns were recorded in the range $2^\circ < 2\theta < 85^\circ$ with a step size 0.015° and a scan speed of 0.3 s/step. The phase identification was based on JCPDF data files. The average size of crystallites was estimated using the Scherrer equation. TEM and HRTEM images were obtained using a JEM-2100 transmittance electron microscope operating at 200 kV. Aluminas were suspended in water in an ultrasonic bath and then a small droplet deposited onto a TEM copper grid coated with carbon film.

The acidity of the Al_2O_3 samples was measured by temperature programmed desorption of ammonia (NH_3 -TPD). In a typical experiment, an appropriate amount of catalyst to result in a common SSA of ca. 30 m^2 for all samples (e.g., 150 mg for Al4) was placed in a quartz reactor (6 mm I.D.) and held in place by means of quartz wool. Prior to adsorption of ammonia, the sample was heated at 450 °C under flowing He for 15 min to remove adsorbed species from the catalyst surface, treated with 20% O_2 (in He) at 300 °C for 30 min, purged with He at 450 °C for 15 min and subsequently

Table 1

Textural characteristics, average particle size and ammonia uptake of the studied catalysts, and apparent activation energies (E_a) for the methanol dehydration reaction.

Catalyst	Notation	SSA ($\text{m}^2 \text{ g}^{-1}$)		Pore volume Used ($\text{cm}^3 \text{ g}^{-1}$)	Pore size Used (nm)	Average particle size		NH_3 uptake ($\mu\text{mol g}^{-1}$)	E_a (kcal mol $^{-1}$)
		Fresh catalyst	Used catalyst			Fresh (nm)	Used (nm)		
α - Al_2O_3 Alfa Products	Al1	<0.5	<0.5	–	–	–	–	–	18.5
γ - Al_2O_3 , Alfa Products	Al2	94	91	0.25	8.6	7.1 ± 0.1	7.1 ± 0.1	227	25.1
γ - Al_2O_3 Houdry	Al3	139	132	0.30	7.2	8.3 ± 0.1	8.2 ± 0.1	293	26.2
γ - Al_2O_3 Engelhard	Al4	202	200	0.78	12.5	5.2 ± 0.1	5.4 ± 0.1	443	27.0
γ - Al_2O_3 (94.6%) Sasol Puralox	Al5	196	193	0.58	9.8	5.4 ± 0.1	5.1 ± 0.1	486	29.8
γ - Al_2O_3 Akzo, treated	Al6	232	224	0.65	9.2	4.7 ± 0.1	5.1 ± 0.1	608	21.4
Al_2O_3 (home made) sol-gel, method 1	SG1	346	304	2.13	22.7	3.4 ± 0.1	3.3 ± 0.1	886	24.1
Al_2O_3 (home made) sol-gel, method 2	SG2	160	139	0.16	3.8	–	2.6 ± 0.1	438	19.5

cooled down to room temperature under flowing He. The flow was then switched to 0.5% NH₃ (in He) for 30 min. Finally, the system was purged with flowing He (30 cm³ min⁻¹) for 15 minutes to remove gas-phase and weakly adsorbed ammonia, and the temperature was increased linearly from 25 to 500 °C with a heating rate of 30 °C min⁻¹. The desorption process was monitored by a mass spectrometer (Omnistar/Pfeiffer Vacuum) connected on line with the reactor outlet.

2.2. Temperature-programmed experiments with mass spectrometry

Adsorption–desorption characteristics and reactivity of methanol were investigated with the use of temperature-programmed desorption (TPD) and temperature-programmed surface reaction (TPSR) techniques coupled with mass spectrometry (MS). In a typical experiment, a pre-weighed amount of catalyst (100 mg) was placed in a quartz microreactor (6 mm I.D.), heated under He flow at 450 °C for 15 min to remove adsorbed species from the catalyst surface and subsequently cooled down to room temperature. The feed was then switched to a 0.5% CH₃OH (in He) mixture (30 cm³ min⁻¹) for 30 min, by controlling the flow of two independent He lines, one of which passed through a saturator containing liquid methanol. The concentration of methanol at the exit of the saturator was estimated by the vapor pressure of methanol at room temperature. For TPD-MS experiments, the system was then purged with He flow (30 cm³ min⁻¹) for 10 min and temperature was increased linearly ($\beta = 15 \text{ }^{\circ}\text{C} \text{ min}^{-1}$) up to 500 °C. TPSR-MS experiments were performed in a similar manner, with the exception that linear heating was performed under flowing 0.5% CH₃OH (in He) mixture.

An Omnistar/Pfeiffer Vacuum mass spectrometer was used for on-line monitoring of effluent gas composition. The transient-MS signals at $m/z = 2$ (H₂), 15 (CH₄), 18 (H₂O), 28 (CO), 31 (CH₃OH), 45 (CH₃OCH₃) and 44 (CO₂) were continuously recorded. Responses of the mass spectrometer were calibrated against self-prepared mixtures of accurately known composition.

2.3. In situ FTIR spectroscopy

Fourier transform infrared (FTIR) experiments were carried out using a Nicolet 6700 apparatus equipped with a diffuse reflectance (DRIFT) cell (Spectra Tech), an MCT detector and a KBr beam splitter. The gas inlet of the cell was directly connected to a flow system equipped with mass flow controllers, two temperature-controlled saturators containing methanol and water, respectively, and a set of valves which allowed selection and control of feed gas composition. The He streams, which passed through the saturators, were mixed with another He stream to give the desired feed composition. In a typical experiment, the catalyst powder was first treated at 450 °C under He flow for 10 min and subsequently cooled down to room temperature (RT) under He flow. During the cooling stage, background spectra were collected at temperatures of interest.

In situ TPD-DRIFTS experiments were performed following interaction of the pretreated Al₂O₃ sample with a flowing gas mixture consisting of either 1.5% H₂O (in He) or 0.5% CH₃OH (in He) at 25 °C for 30 min, purging with He for 30 min, and subsequent stepwise heating (with 50 °C increments) under He flow up to 450 °C. The same procedure was followed to investigate the reactivity of methanol in the presence and in the absence of water in the feed (TPSR-DRIFTS experiments), with the exception that interaction of the catalyst with 0.5%CH₃OH (in He) or 1.5% H₂O + 0.5% CH₃OH (in He) at 25 °C for 30 min was followed by heating under a flow of the same reaction mixture. Spectra were recorded after reaching the

desired temperature at a resolution of 4 cm⁻¹. In all experiments, the total flow rate through the DRIFT cell was 30 cm³ min⁻¹.

2.4. Catalytic performance tests and kinetic measurements

The apparatus used for catalytic performance tests and kinetic measurements comprises the reactor, a flow measuring and control system and an on line analysis system. The reactor consists of a 25-cm long quartz tube (6 mm O.D.) with an expanded 1-cm long section in the middle (8 mm I.D.), in which the catalyst sample is put and kept in place by means of quartz wool. Reaction temperature is measured in the middle of the catalyst bed by means of a K-type thermocouple placed within a quartz capillary well, which runs through the cell. The reactor is placed in an electric furnace, the temperature of which is controlled by a second K-type thermocouple placed between the reactor and the walls of the furnace. The flow system is equipped with a set of mass-flow controllers (MKS) to control the flow and composition of the inlet gases (He in the present case), a syringe pump (Braintree Scientific Inc.), which is used for feeding methanol or methanol–water mixtures, a pressure indicator to measure the pressure drop in the catalyst bed and a set of valves, which allow introduction of the gas mixture to the reactor or to a by-pass loop stream. Methanol (or methanol–water mixture) is pumped into a vaporizer heated at 170 °C and mixed with the He stream coming from the mass-flow controller. The resulting gas mixture is then fed to the reactor through stainless steel tubing maintained at 150 °C by means of heating tapes. The analysis system consists of a gas chromatograph (Shimadzu) interfaced to a personal computer. The chromatograph is equipped with two packed columns (Porapak-Q, Carbovax) and two detectors (TCD, FID) and operates with He as the carrier gas. The injection of the gas mixture to the desired column is achieved by means of two six-port valves heated at 150 °C. Determination of the response factors of the detectors has been achieved with the use of gas streams of known composition. Helium gas is supplied from a high-pressure gas cylinder (Messer Griesheim GMBH) and is of ultra-high purity.

Catalytic performance was investigated in the temperature range of 150–400 °C using a feed composition consisting of 30% CH₃OH (in He). When water was added in the feed, part of the balance gas (He) was replaced by water vapor (10% H₂O). In a typical experiment, an amount of 400 mg of fresh catalyst (0.18 < d < 0.25 mm) was placed in the reactor, heated at 400 °C under He flow and left at that temperature for 1 hour. The flow was then switched to the reaction mixture, the catalyst was conditioned under reaction conditions at 400 °C for 30 min, and the concentrations of reactants and products at the reactor effluent were determined using the analysis system described above. Similar measurements were obtained following a stepwise lowering of temperature until conversion of CH₃OH dropped close to zero. A few more measurements were then made by stepwise increase of temperature to check for possible catalyst deactivation. In all cases, measurements were obtained after the system had reached steady state conditions and data points presented are averages of at least three measurements. Experiments were conducted at near atmospheric pressure under a total flow rate of 30 cm³ min⁻¹, which corresponds to a gas hourly space velocity (GHSV) of 2500 h⁻¹.

Kinetic measurements were performed in separate experiments where the conversion of methanol was kept below 15% so that differential reaction conditions could be assumed, with negligible heat and mass transfer effects. Reaction rates were calculated using the following expression:

$$r_{\text{MeOH}} = \frac{(C_{\text{MeOH}}^{\text{in}} - C_{\text{MeOH}}^{\text{out}})F}{W} \quad (5)$$

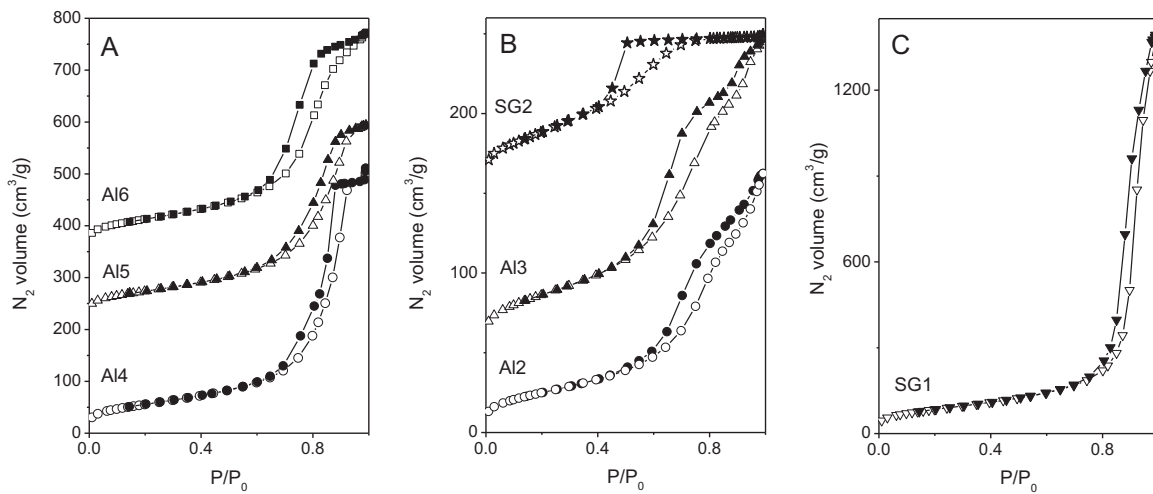


Fig. 1. The N₂ adsorption/desorption isotherms of the studied Al₂O₃ samples. The hollow and solid symbols denote N₂ adsorption and desorption, respectively. (A) The isotherms for samples Al4, Al5 and Al6 were offset vertically by 0, 220 and 350 cm³ g⁻¹ (STP), respectively; (B) the N₂ isotherms for samples Al2, Al3 and SG2 were offset vertically by 0, 50 and 150 cm³ g⁻¹ (STP), respectively; (C) N₂ adsorption/desorption isotherms of SG1.

where r_{MeOH} is the conversion rate of methanol (mol s⁻¹ g_{cat}⁻¹), F is the total flow rate (mol s⁻¹), W the mass of catalyst (g) and $C_{\text{MeOH}}^{\text{in}}, C_{\text{MeOH}}^{\text{out}}$, are the inlet and outlet concentrations of methanol, respectively.

3. Results and discussion

3.1. Physicochemical characteristics of Al₂O₃ catalysts

Results of catalyst characterization showed that the textural characteristics of the fresh catalysts vary significantly from one sample to another. In particular, specific surface area varies from less than 0.5 m² g⁻¹ for α -Al₂O₃ (Al1) to 346 m² g⁻¹ for Al₂O₃ prepared by sol-gel method (SG1) (Table 1). Among the studied samples, SG1 exhibits the highest SSA, the highest pore volume and the highest average pore diameter. The textural analysis of the used catalysts showed that exposure to reaction conditions did not alter appreciably SSA of commercial catalysts (samples A1 to Al6), but was more important for self-prepared materials, namely SG1 and SG2 (Table 1).

The nitrogen adsorption/desorption isotherms of all used samples were found to be similar to those of the fresh catalysts shown in Fig. 1, and can be classified into three main groups. For Al4, Al5 and Al6 samples, the classical type IV isotherm (according to the IUPAC classification) can be observed, typical for mesoporous solids (Fig. 1A). The type H1 hysteresis loop, occurring at the relative pressure range of $P/P_0 = 0.7$ –0.9, indicates broad pore size distribution with uniform cylindrical shape [44,45]. The pore size distribution shown in Fig. 2 confirms the mesoporous structure of Al4, Al5 and Al6 with an average pore width of about 10 nm, while larger pores of about 17.3 nm are also measured for Al4. The calculated average pores' size, given in Table 1, confirms this observation. The Al2 and Al3 samples exhibit quite different isotherms having two inflection points, which implies non uniform pores' shape and lower porosity (Fig. 1B). The calculated mean diameter of the pores is also smaller for these two aluminas (Table 1). The BJH analysis has shown that Al1 is a non porous material, as expected for a α -Al₂O₃ sample (not shown).

The two home-made aluminas are very different from one another but also very different from all commercial samples investigated. The N₂ adsorption/desorption isotherm for SG1 (Fig. 1C) resembles a type II with almost no plateau at high P/P_0 values, usually observed for materials with macropores or interparticular

mesoporosity [46]. This type of isotherms, which is characteristic of clay minerals, suggests N₂ physisorption between aggregates of platelet particles giving rise to slit-shaped pores [47]. The hysteresis loop appearing at higher relative pressure, compared to the other aluminas, indicates larger mesopores. Thus, from this isotherm (Fig. 1C) high porosity, large pores with uniform size and shape is expected for SG1. Indeed the average pore diameter has been calculated to be 22.7 nm and the total porosity 2.13 cm³ g⁻¹, i.e., much higher than those of any other material studied. On the contrary, SG2 shows a type IV isotherm and H2 hysteresis, attributed to nonuniform size and/or ink bottle shape (Figs. 1B and 2) [44,45]. SG2 has much lower porosity and pores (Table 1), the pore size distribution indicating the existence of micropores (Fig. 2).

The XRD patterns of the fresh samples reveal that the materials consist mainly of γ -Al₂O₃ (Fig. 3). However, the width of the peaks varies, demonstrating differences in crystallinity. Sample Al3 exhibits sharp peaks, signifying larger crystallites' size while samples prepared by the sol-gel methods give very broad diffraction bands due to the poor intrinsic crystallization of the alumina. For sample Al2, multiple peaks are clearly observed, implying that crystallographic phases other than γ -Al₂O₃ are also present, probably δ -Al₂O₃ and χ -Al₂O₃. Preparative conditions and thermal

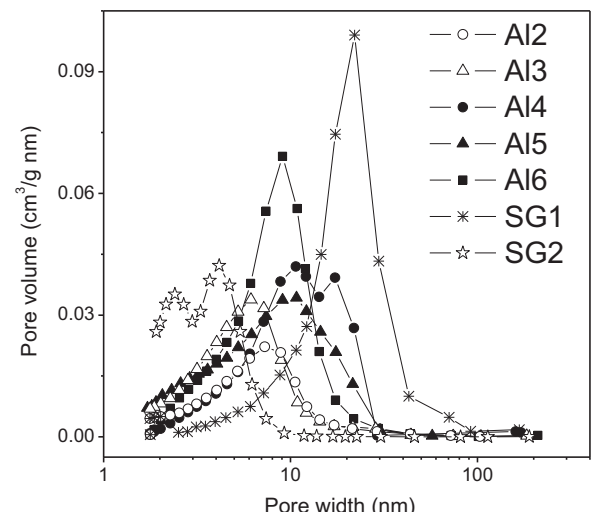


Fig. 2. Pore size distribution of the studied Al₂O₃ catalysts.

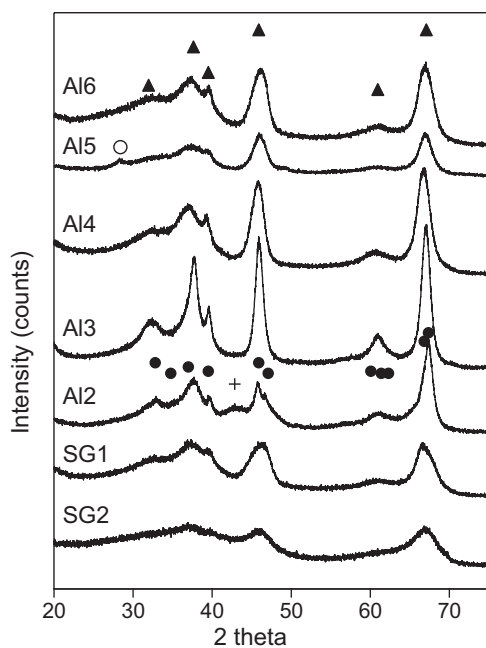


Fig. 3. X-ray diffraction (XRD) patterns obtained over the indicated Al_2O_3 catalysts. Symbols correspond to the following JPCS data: ▲ 10-0425 γ - Al_2O_3 , ● 04-0877 δ - Al_2O_3 , + 04-0880 χ - Al_2O_3 , ○ 21-1307 $\text{Al}(\text{OH})$.

treatment define the extent of hydroxyls incorporation and structural rearrangements resulting in the formation of various transition aluminas [48]. The detection of χ - Al_2O_3 indicates that gibbsite was present in the precursor oxyhydroxide, while the presence of δ - Al_2O_3 is due to heating above 750 °C. It is worth noting that slight shifts are observed for the other samples, indicative of differences in the lattice parameters and/or the presence of other transition aluminas, especially in the case of SG1. In the XRD pattern of the fresh Al5, the presence of aluminum oxide hydroxide ($\text{Al}(\text{OH})$, JPCS 21-1307) was also detected, with most intense peaks at 14.5° (not shown) and 28.2°. After catalytic tests this phase is absent, indicating that water is removed under reaction conditions. For the other aluminas there are not any remarkable changes observed after catalytic tests (XRD patterns not shown). The degree of crystallization, expressed by the average crystallites size, is shown in Table 1. It can be seen that the average particle size varies, being smaller for the home made SG materials. In accordance, the samples with smaller crystallites exhibit higher SSAs. No increase of the particles' size is observed for the used catalysts, confirming the stability of the materials under reaction conditions.

The TEM images of Al_2O_3 samples investigated (cf. Supplementary information, Figs. SI 1 and SI 2) show that Al4 consists of small uniform aggregates of almost spherical shape whereas Al5 presents elongated aggregates of about 20–40 nm. In Al6, the particles have needle-like shape morphology. SG1 seems similar to Al6 with shorter and thinner needles. However, the two materials are quite different. Al6 is well crystallized as it can be seen in the HRTEM images (Fig. SI 2a). On the contrary, a large part of SG1 is amorphous (Fig. SI 2b). Al5 also presents amorphous areas but to a much lower degree. These results are in accordance with the XRD analysis that shows the lower crystallinity of the SG1 as compared to the commercial aluminas.

The acidity of Al_2O_3 catalysts (except the low-SSA α - Al_2O_3 sample) was estimated with temperature programmed desorption of ammonia, which may provide information on both the concentration and strength of acid sites [49]. Ammonia is a suitable probe molecule for this purpose because of its strong basicity, its ability to adsorb selectively on sites of different strengths and its

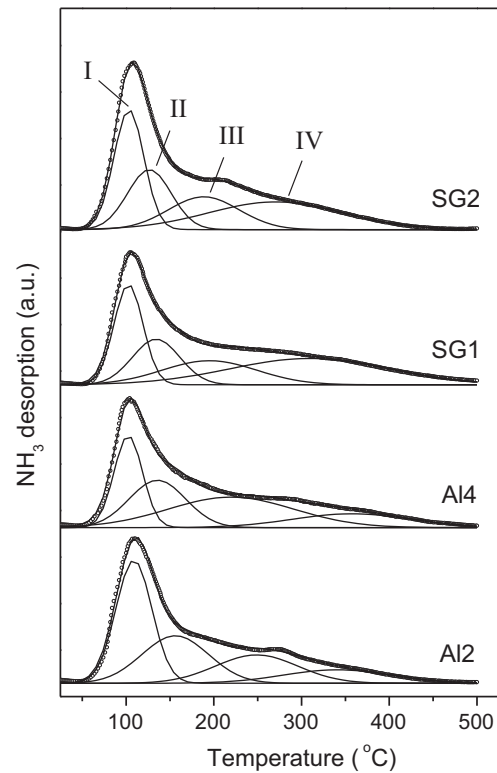


Fig. 4. NH_3 -TPD profiles obtained over the indicated Al_2O_3 catalysts.

small kinetic diameter (0.26 nm), which allows detection of acidic sites located into very narrow pores [49,50]. Typical NH_3 -TPD patterns obtained for Al2, Al4, SG1 and SG2 catalysts are shown in Fig. 4. It is observed that, in all cases, TPD patterns are characterized by an intense desorption peak located at ca. 105 °C and a broad asymmetric decaying “tail” which extends up to ca. 500 °C. Qualitatively similar NH_3 -TPD profiles are typically observed for different crystalline phases of Al_2O_3 [41,51,52]. It should be noted that no other products, such as H_2 or N_2 , were detected during adsorption/desorption experiments, indicating that adsorption and desorption of ammonia on the present materials take place molecularly. The total amounts of NH_3 desorbed per gram of catalyst are listed in Table 1. It is observed that the NH_3 uptake per gram of catalyst depends strongly on specific surface area of the sample, and increases linearly with increase of SSA (Fig. 5). If the same data are expressed per unit surface area, the density of surface acid sites is

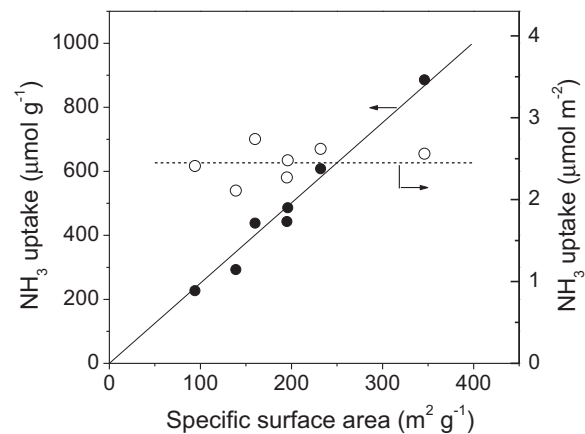


Fig. 5. Amount of ammonia desorbed in NH_3 -TPD experiments as a function of the specific surface area of Al_2O_3 catalysts.

approximately the same for all samples, taking an average value of $\text{ca. } 2.45 \mu\text{mol m}^{-2}$ (Fig. 5).

The NH_3 -TPD patterns of Fig. 4 show that ammonia is adsorbed on the surface of Al_2O_3 catalysts with different strengths. Since the catalytic activity of solid acids for methanol dehydration depends on both the number and strength of acid sites, an attempt has been made to elucidate the type of acid sites present on each sample. For this, the NH_3 -TPD profiles were deconvoluted into Gaussian peaks, on the assumptions that (a) the activation energy of desorption (E_d) is constant and independent of surface coverage, and (b) a normal distribution of E_d arises from a corresponding heterogeneity of sites distribution [49]. The fitting procedure showed that all experimental curves may be deconvoluted into (at least) four peaks with their maxima located at $104 \pm 4^\circ\text{C}$ (peak I), $135 \pm 14^\circ\text{C}$ (peak II), $205 \pm 32^\circ\text{C}$ (Peak III) and $322 \pm 36^\circ\text{C}$ (peak IV) (Fig. 4). Peaks I and II may be attributed to desorption of NH_3 from weak acid sites, whereas peaks III and IV correspond to medium and strong acid sites, respectively [42,49,50,53–55]. The exact nature of the adsorption sites (Brønsted or Lewis) corresponding to the four TPD peaks cannot be concluded from the present results. It has been proposed that the peak at 105°C may be attributed to Brønsted acid sites and the peaks at higher temperature to Lewis sites [50].

3.2. Catalytic performance tests and kinetic studies

3.2.1. Thermodynamic analysis

Thermodynamic analysis of the methanol dehydration reaction (4) has been carried out using the Outokumpu HSC Chemistry® program. Representative results are shown in Fig. 6, where the Gibbs free-energy (ΔG°), entropy (ΔS°) and enthalpy (ΔH°) changes of the reaction are plotted as functions of reaction temperature. It is observed that the reaction is exothermic, with ΔH° and ΔS° decreasing from -23.7 to $-83.7 \text{ kJ mol}^{-1}$ and from -23.9 to -98.9 kJ K^{-1} , respectively, with increasing temperature in the range of $0– 750°C . The reaction is not favored thermodynamically at temperatures higher than 525°C , where ΔG° takes positive values. The equilibrium constants determined are in good agreement with those reported in the literature [56] and were used to calculate the equilibrium conversion of methanol as a function of temperature for the feed compositions used in the present study (Figs. 7 and 10, *vide infra*).$

3.2.2. Catalytic performance tests

Results of catalytic performance tests obtained over the studied catalysts with the use of a feed composition consisting of 30% CH_3OH (in He) are summarized in Fig. 7 where the conversion

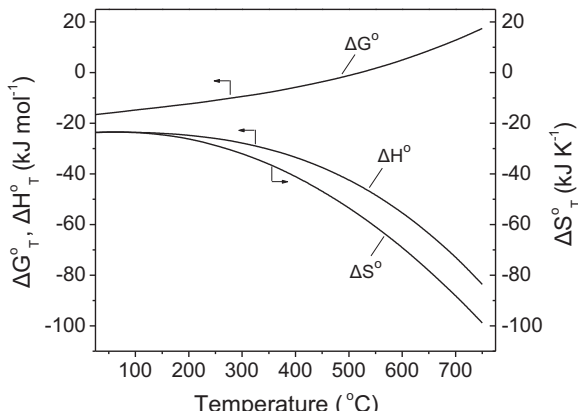


Fig. 6. Entropy (ΔS), Gibbs free energy (ΔG) and enthalpy (ΔH) changes of methanol dehydration to dimethyl ether reaction as functions of reaction temperature.

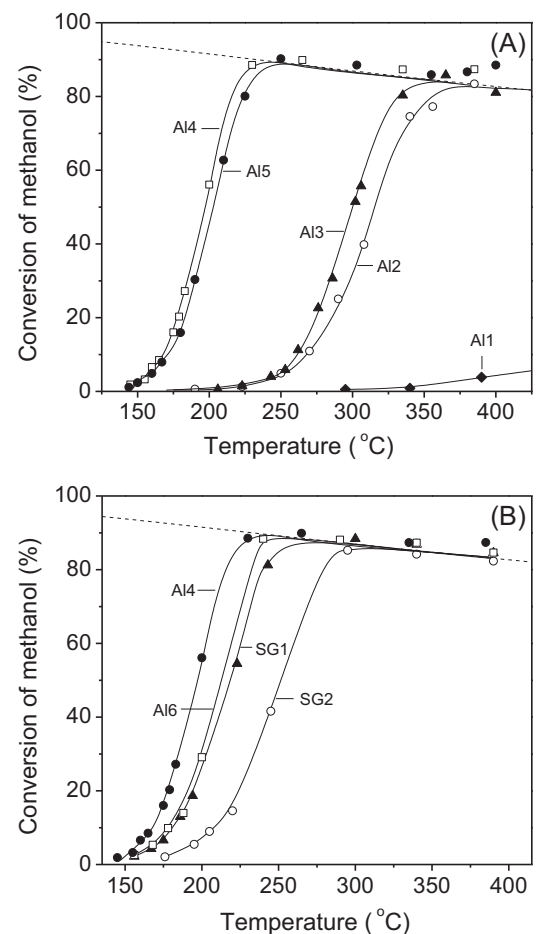


Fig. 7. Conversion of methanol as a function of reaction temperature obtained over (A) commercial (Al1–Al5) and (B) pretreated (Al6) and home-made Al_2O_3 catalysts synthesized with sol-gel (SG1, SG2); The conversion curve obtained over the best performing catalyst (Al4) is shown in both graphs, for comparison. The equilibrium conversion curve is shown with dashed line. Experimental conditions: feed composition: 30% CH_3OH (in He); mass of catalyst: 400 mg; total flow rate: $30 \text{ cm}^3 \text{ min}^{-1}$.

of methanol (X_{MeOH}) is plotted as a function of reaction temperature. The equilibrium conversion curve for methanol dehydration to DME (reaction (4)) is also shown, for comparison. As observed in Fig. 7A, the Al1 catalyst is, practically, inactive in the temperature range of interest. This should be expected, because of the very low SSA of α - Al_2O_3 (Table 1). Samples Al2 and Al3, with SSAs of $\text{ca. } 90$ and $130 \text{ m}^2 \text{ g}^{-1}$, respectively, exhibit measurable methanol conversion at temperatures higher than 200°C and reach equilibrium conversion at around 350°C . The methanol conversion curve shifts toward significantly lower temperatures over samples Al4 and Al5 with SSAs around $190 \text{ m}^2 \text{ g}^{-1}$, exhibiting significant activity at temperatures lower than 200°C and reaching equilibrium conversions at temperatures around 230°C (Fig. 7A). In Fig. 7B are shown similar results obtained over the pretreated commercial alumina sample (Al6) and the self-prepared catalysts synthesized with the use of sol-gel method (SG1, SG2). It is observed that, although Al6 and SG1 are characterized by relatively large SSAs (Table 1), their catalytic activity is inferior, compared to that of the best performing Al4 sample.

Regarding selectivity to reaction products, typical results obtained over the Al4 sample are shown in Fig. 8, where selectivities to DME (S_{DME}), carbon monoxide (S_{CO}) and methane (S_{CH_4}) are plotted as functions of reaction temperature. It is observed that the catalyst is 100% selective toward DME in the temperature range of 150 to $\text{ca. } 325^\circ\text{C}$. At higher temperatures, small amounts

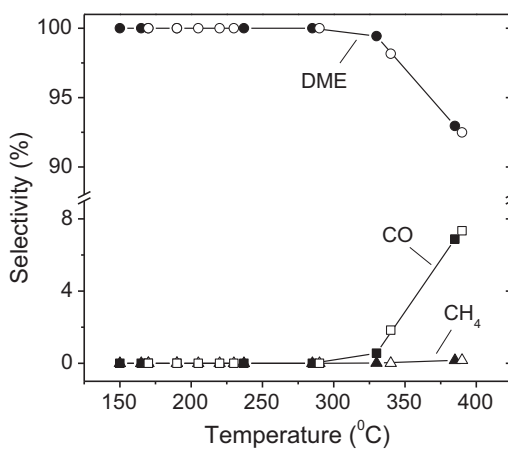


Fig. 8. Selectivities to reaction products as functions of reaction temperature obtained over the Al4 sample using a feed composition consisting of 30% CH₃OH (closed symbols) or 30% CH₃OH + 10% H₂O (open symbols). Other conditions same as in Fig. 7.

of CO and trace amounts of CH₄ appear in the gas phase. Selectivity toward these species increases progressively with increase of temperature to 400 °C at the expense to that of DME. Similar results were obtained for all Al₂O₃ catalysts investigated. It may be noted that the occurrence of side reactions responsible for the evolution of CO and CH₄ above ca. 325 °C explains the reason why conversion of methanol exceeded the equilibrium values predicted by thermodynamics for reaction (4) in this temperature range (Fig. 7).

3.2.3. Kinetic measurements

Results of kinetic measurements obtained with the use of a feed composition consisting of 30% CH₃OH (in He) are summarized in the Arrhenius plots of Fig. 9A, where the reaction rate is expressed per gram of catalyst. The apparent activation energy (E_a) of the methanol dehydration reaction was calculated from the slope of the fitted lines and results obtained are summarized in Table 1. It is observed that E_a is, practically, the same for all studied catalysts taking an average value of 24 ± 4 kcal mol⁻¹, in agreement with literature results [30].

Results of Fig. 9A show that the rate of methanol conversion per gram of catalyst depends strongly on the nature of the Al₂O₃ sample employed. In particular, the rate at temperatures around 200 °C is more than two orders of magnitude (ca. 200 times) higher for samples Al4 and Al5, compared to that of Al2 and Al3, with other catalysts exhibiting intermediate activity. These differences cannot be explained solely by taking into account differences of the SSA or of the total number of acid sites (determined by NH₃-TPD), which vary only by a factor of 3 for the studied samples (Table 1). This is clearly evidenced in the Arrhenius plots of Fig. 9B, where the reaction rates are divided with the moles of ammonia desorbed per unit mass of catalyst. If the reaction rate was directly proportional to the total number of acidic sites, all data points should fall on the same Arrhenius line, which, obviously, is not the case. Thus, although some authors reported that catalytic activity correlated well with the number of acidic sites of γ -Al₂O₃ [54], no such correlation could be obtained in the present study, in agreement with results of other investigators [51].

Results of Fig. 9 imply that physicochemical characteristics other than SSA or total number of surface acid sites (estimated by NH₃-TPD) determine to a large extent the activity of Al₂O₃ catalysts for the title reaction. It has been reported, for example, that alumina samples with the highest proportion of weak/moderate acid sites exhibit the best catalytic performance and stability for the synthesis of dimethyl ether, and that the variation in activity of

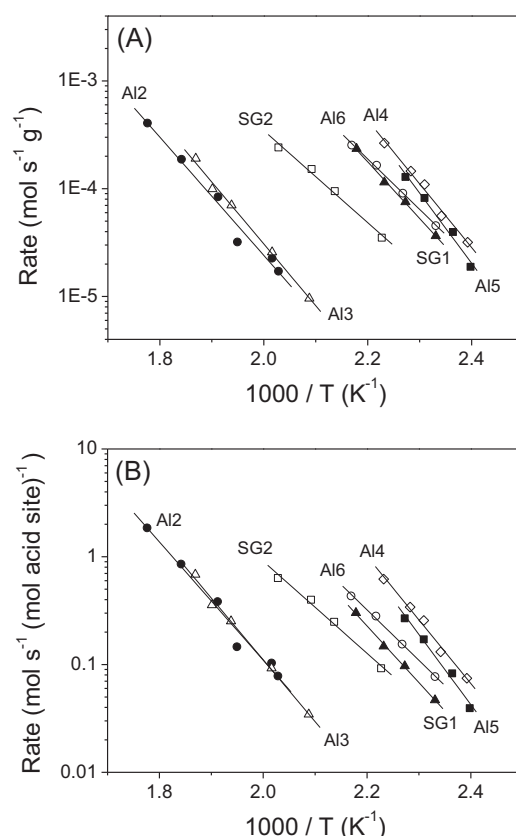


Fig. 9. Arrhenius plots of specific reaction rates obtained over the studied Al₂O₃ samples under differential reaction conditions, expressed (A) per gram of catalyst and (B) per mol of surface acid sites.

Al₂O₃ catalysts is a result of different acidities and ratios of weak-to-strong acidic sites [30,39,42,43]. This explains the reason why catalytic activity can be varied by addition of promoters or by controlling the acidic properties of alumina or zeolites [28,29]. Based on these arguments, an attempt has been made to correlate catalytic activity of the studied samples with the number of weak, medium or strong acid sites estimated by deconvolution of the NH₃-TPD patterns (Fig. 4). Results of this analysis (not shown for brevity) did not show a direct correlation between the amounts of acid sites of different strengths with catalytic activity. This is may be, at least in part, due to the absence of clearly resolved peaks in the NH₃-TPD patterns (Fig. 4), which does not allow accurate determination of the surface concentration of acid sites of various strength. It should be noted that the NH₃-TPD method does not provide information related to the types of acidic sites (e.g., Brønsted or Lewis sites) present on the catalyst surface [51], which have been reported to exhibit different activities [28]. Therefore, the possible effects of the types of acidic sites on catalytic performance are not further discussed here.

The assessment of the textural properties showed that, in addition to SSA, the aluminas differ also in their porosity and average pore diameter. The importance of the pores' structure for dehydration reactions has been reported for materials characterized by microporosity such as zeolites and pillared clays [9,22,57,58]. Methanol dehydration, considered as a bimolecular reaction between two methoxy species or between a methoxy species and an undissociated methanol adsorbed on adjacent surface sites, would require the close proximity of two acid sites with adequate acidity but also pores having size large enough to permit this type of reactions. Even larger pores would be needed if one considers a single dehydration site for the formation of a methoxy

species that would react with a methanol molecule in the gas phase [57]. On the other hand, ammonia is an excellent probe molecule for testing the acidic properties of solid catalysts due to its strong basicity and small molecular size that allow for detection of acidic sites located also into very narrow pores [49]. Thus, acidic sites in narrow pores, although titrated by ammonia, may be ineffective for DME formation due to steric inhibition. Raimondo et al. [57] studied the acidity/porosity relationships on oxide-pillared materials and proposed that dehydration is favored in large pores. Even though the above restrictions should not apply in the case of mesoporous materials such as aluminas, the results of the present study indicate that catalysts with cylindrical pores of an average width of about 9–10 nm and total porosity 0.60–0.80 cm³ g⁻¹ exhibit higher methanol conversion than those with lower porosity. Further porosity increase (SG1) does induce additional activity enhancement. Comparable results have also been reported over similar materials for the title reaction [59].

Another parameter that can affect catalytic behavior is the degree of crystallinity of the materials. The XRD patterns (Fig. 3) and the TEM images (cf. Supplementary Information, Figs. SI 1 and SI 2) revealed differences in the crystallinity of the alumina samples. Having in mind that smaller crystallites signify higher number of defects and therefore of methanol adsorption sites, the decrease of particle size of Al₂O₃ should be accompanied by an analogous increase in methanol conversion. This is true when the crystallites' size decrease from 7.0–8.0 nm (Al2 and Al3) to about 5.0–5.5 nm (Al4, Al5, Al6). Further decrease of crystallites size, as in the case of SG1 does not result in additional increase of the activity. However, this material is highly amorphous.

Based on the above discussion, it may be concluded that the textural properties, degree of crystallinity and total amount of acid sites determine to a large extent the catalytic behavior of the studied Al₂O₃ catalysts for the dehydration of methanol to dimethyl ether.

3.2.4. Effects of the presence of water vapor in the feed

Under realistic reaction conditions, where methanol is produced via hydrogenation of CO and/or CO₂, the gas mixture contains considerable amounts of water steam, which may influence the activity and stability of the methanol dehydration catalyst. In order to address this issue, the effects of the presence of 10% water vapor in the feed on catalytic performance have been investigated over the Al4 sample and results are shown in Fig. 10. It is observed that the presence of water decreases substantially catalytic activity, which is evidenced by a shift of the methanol conversion curve toward higher temperatures by ca. 50 °C (Fig. 10A). This is accompanied by an increase of the apparent activation energy of the reaction from 27 to 37 kcal mol⁻¹, in good agreement with results of previous studies [30]. Interestingly, the presence of water in the feed does not influence selectivity to reaction products (Fig. 8).

In Fig. 10B is shown the variation of the conversion of methanol (X_{MeOH}) with time-on-stream obtained over the Al4 sample at a constant temperature of 215 °C, in the absence and in the presence of water in the feed. It is observed that, when a 30%CH₃OH (in He) mixture is fed to the reactor, the catalyst exhibits a very stable performance with the conversion of methanol acquiring values around 60%. Addition of 10% H₂O in the feed results in a substantial decrease of methanol conversion. However, catalytic activity is restored when water is removed from the feed and X_{MeOH} returns to its initial value. This clearly shows that the effect of water on catalytic performance is reversible.

Results of Fig. 10 show that Al4 deactivates in the presence of water. This behavior, which is typically observed for solid acid catalysts [30,42], is believed to be due to blocking of the active sites for methanol conversion via competitive adsorption of water on the catalyst surface [30,40,42,60]. These issues are discussed in more

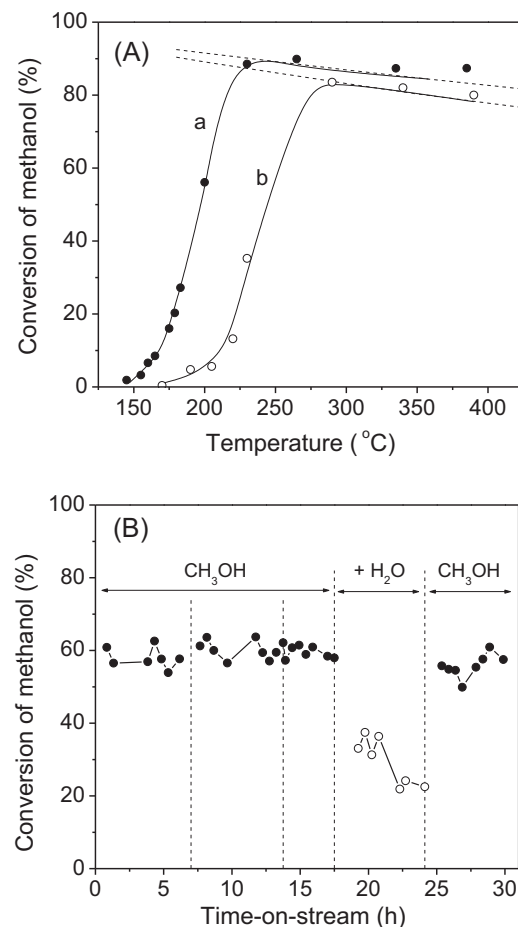


Fig. 10. (A) Conversion of methanol as a function of reaction temperature obtained over Al₂O₃ catalyst (Al4 sample) (a) in the absence and (b) in the presence of 10% H₂O in the feed. (B) Effect of addition of 10% H₂O in the feed on the conversion of methanol at $T=215^{\circ}\text{C}$.

detail in the following section. It should be noted that the presence of water in the feed shifts equilibrium of reaction (4) to the left and, therefore, part of the observed decrease of methanol conversion is due to thermodynamic reasons (see, for example, dashed lines in Fig. 10A). Thus, when water is present in the reaction mixture, a higher reaction temperature is always required to achieve the same level of conversion. In practice, the negative effect of water can be suppressed if the one-step syngas-to-DME hybrid catalyst contains a component, which is active for the WGS reaction, in which case excess water may be removed efficiently [30].

3.3. Mechanistic studies

The nature, relative population, thermal stability and reactivity of species formed on the catalyst surface under reaction conditions have been investigated with the use of *in situ* DRIFTS and transient-MS techniques, following interaction of Al₂O₃ (Al4) with either (a) 1.5% H₂O (in He) or (b) 0.5% CH₃OH (in He) or (c) 1.5% H₂O + 0.5% CH₃OH (in He) mixtures.

3.3.1. Adsorption/desorption characteristics of water

In Fig. 11A are shown DRIFT spectra obtained following exposure of the Al₂O₃ catalyst to a 1.5% H₂O (in He) mixture at 25 °C for 30 min, switch to He flow for 30 min (trace a) and subsequent step-wise heating at 450 °C under He flow (traces b–i). It is observed that the spectrum obtained at 25 °C (trace a) is characterized by two absorption bands located at 1645 and 1390 cm⁻¹, a broad

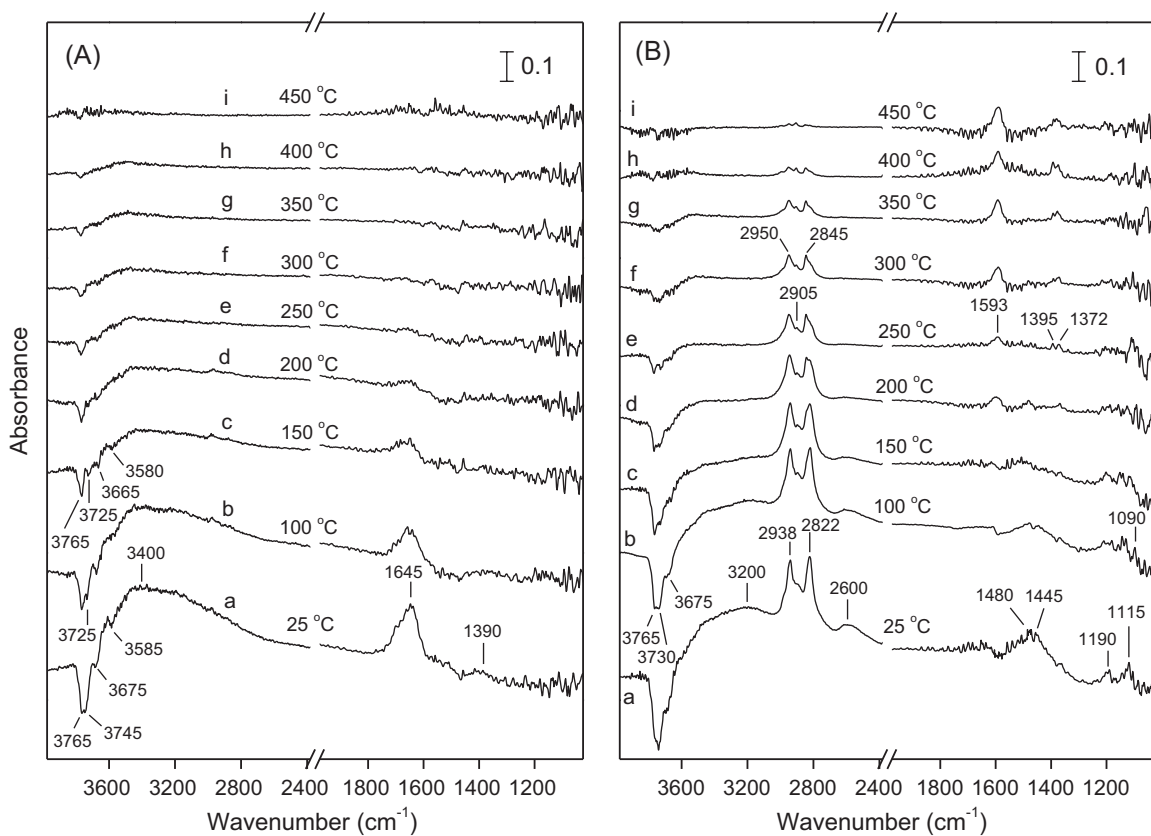


Fig. 11. DRIFT spectra obtained over the Al_2O_3 (Al4) catalyst following interaction with (A) 1.5% H_2O (in He) or (B) 0.5% CH_3OH (in He) at 25 °C for 30 min and subsequent stepwise heating at the indicated temperatures under He flow.

feature in the 3500–2800 cm^{-1} region and several overlapping, negative peaks in the 3800–3500 cm^{-1} region. The intense band at 1645 cm^{-1} can be assigned to the $\delta(\text{HOH})$ bending vibrations of weakly (physically) adsorbed water, whereas the weak band at 1390 cm^{-1} can be attributed to the same vibration of water molecules adsorbed on coordinatively unsaturated aluminum ions [61,62]. The latter adsorption sites could have been formed during pretreatment of the sample at 450 °C under He flow, which is known to result in partial dehydroxylation of the Al_2O_3 surface [61,63]. The broad band in the 3500–2800 cm^{-1} region contains contributions of $\nu(\text{OH})$ vibrations originating from various species, including weakly adsorbed water molecules, hydrogen-bonded hydroxyl groups, and shifted $\nu(\text{OH})$ vibrations of alumina surface caused by interaction with adsorbed water [64].

Regarding the “negative” bands observed in the range of 3800–3500 cm^{-1} , they appear in the region where the $\nu(\text{OH})$ stretching vibrations of various configurations of hydroxyl groups of alumina are expected to occur [61,63]. The loss of intensity observed in this region upon exposure to water vapor indicates that hydroxyl groups initially present on the Al_2O_3 surface interact with adsorbed water molecules [62,64], and that this interaction results in a shift of absorption toward lower wavenumbers (increased intensity in the 3500–2800 cm^{-1} region). It may be noted that, according to the analysis of Knozinger and Ratnasamy [63], a maximum of five different OH configurations are expected to be present on the surface of aluminas, their actual occurrence and relative concentration depending on the relative contributions of the different crystal phases. These configurations may be tentatively correlated to the five (negative) spectral features located at ca. 3765, 3745, 3725, ~3670 and ~3585 cm^{-1} (Fig. 11A, traces a–c).

Stepwise increase of temperature under He flow results in a progressive decrease of the intensities of the bands located at

1645, 1390 and 3500–2800 cm^{-1} (traces b–i). These spectral features disappear at temperatures higher than ca. 250 °C, indicating desorption of physically adsorbed and coordinatively bonded water molecules [62]. This is accompanied by the progressive disappearance of the negative bands in the 3800–3500 cm^{-1} region and the restoration of the coverage of hydroxyl groups on the alumina surface.

3.3.2. Temperature programmed desorption of methanol

The TPD pattern obtained following interaction of Al_2O_3 (Al4) with 0.5% CH_3OH (in He) at 25 °C is shown in Fig. 12A. It is observed that desorption of methanol starts at room temperature and goes through a maximum at 105 °C. This indicates that a substantial amount of methanol is weakly held on the catalyst surface and desorbs in the gas phase according to:



DME starts to evolve at temperatures around 150 °C, goes through a maximum at ca. 210 °C and is present at the reactor effluent at temperatures as high as 400 °C. At temperatures higher than 325 °C, CO, H_2 and CH_4 start to evolve in the gas phase and their concentrations reach a maximum at around 420 °C. Desorption of all products is completed below 550 °C.

Results of Fig. 12A show that Al_2O_3 (Al4) is able to selectively dehydrate methanol toward DME at temperatures lower than ca. 350 °C, in agreement with results presented in Fig. 8. At higher temperatures, adsorbed species are decomposed toward almost equal amounts of CH_4 , H_2 and CO (Fig. 12A). This indicates that the overall reaction that takes place at temperatures above 350 °C may be described as decomposition of DME:



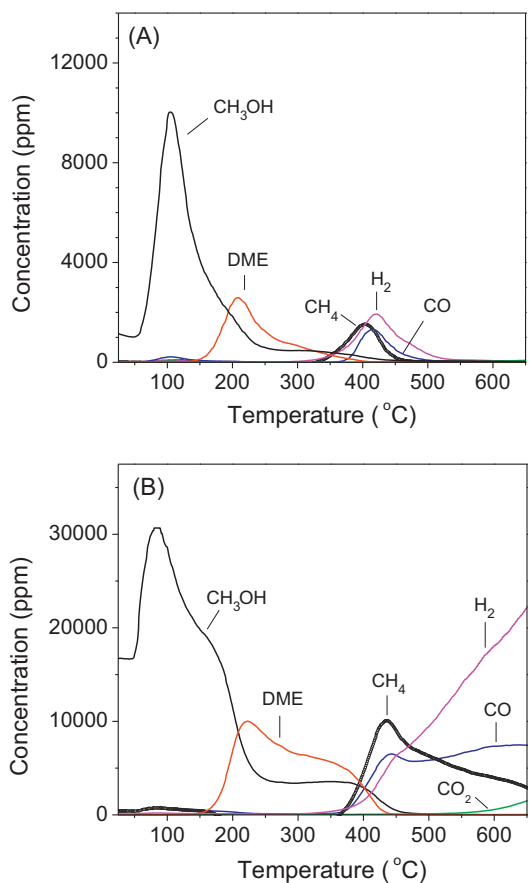
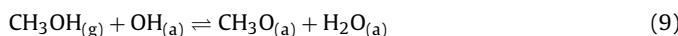
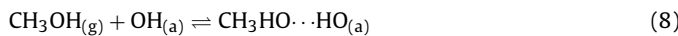


Fig. 12. (A) TPD pattern obtained over the Al_2O_3 (Al4) catalyst following interaction with 0.5% CH_3OH (in He) at 25 °C for 30 min and subsequent linear heating ($\beta = 15^\circ\text{C min}^{-1}$) under He flow; (B) TPSR pattern obtained over the Al_2O_3 (Al4) catalyst following interaction with 1.5% CH_3OH (in He) at 25 °C for 30 min and subsequent linear heating ($\beta = 15^\circ\text{C min}^{-1}$) under a flow of the same gas mixture.

A similar experiment was conducted with the use of DRIFTS in order to investigate the nature and reactivity of species formed on the catalyst surface. Results of this DRIFTS-TPD experiment are presented in Fig. 11B, which shows spectra obtained following interaction of Al_2O_3 with 0.5% CH_3OH (in He) at 25 °C for 30 min, purging with He for 30 min (trace a), and subsequent stepwise heating (with 50 °C increments) at 450 °C under He flow (traces b–i). It is observed that the (background-subtracted) spectrum recorded at 25 °C (trace a) is characterized by negative bands in the $\nu(\text{OH})$ region (3800–3500 cm⁻¹) as well as by several bands in the C–H stretching frequency region (3100–2700 cm⁻¹) and in the C–H deformation and C–O stretching regions (1600–1050 cm⁻¹). Two weak, broad bands can be also discerned at ca. 3200 and 2600 cm⁻¹.

As discussed above, the negative bands located at ca. 3765, 3730 and 3675 cm⁻¹ can be attributed to losses of $\nu(\text{OH})$ intensity of (at least) three different types of free hydroxyl groups initially present on the Al_2O_3 surface. These groups are known to hydrogen-bond to adsorbed methanol and methoxy ($\text{CH}_3\text{O}-$) species, thereby resulting in the appearance of “negative” bands in the $\nu(\text{OH})$ region [65–70]:

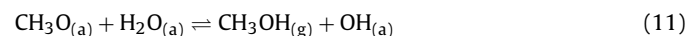
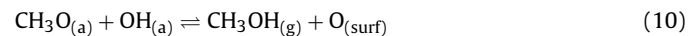


Based on literature results [71], the “negative” spectral features observed in the $\nu(\text{OH})$ region can be assigned to medium-strong (3765 cm⁻¹), medium-weak (3730 cm⁻¹) and weak (3675 cm⁻¹) Lewis acid sites of Al_2O_3 .

The variety of bands observed below 3200 cm⁻¹ (trace a) can be attributed to adsorbed methanol and/or methoxy groups as follows: The intense peaks in the $\nu(\text{C–H})$ region, located at 2938 and 2822 cm⁻¹, can be assigned to the $\nu_{\text{as}}(\text{CH}_3)$ and $\nu_{\text{s}}(\text{CH}_3)$ modes, respectively, of adsorbed methanol/methoxy species [72,73]. A second pair of peaks, located at ca. 2950 and 2845 cm⁻¹, which appear as shoulders at low temperatures (traces a–c) but are clearly resolved at higher temperatures (e.g., traces d–i), can be attributed to similar species bonded more strongly on the Al_2O_3 surface [67]. The broad band observed between 1550 and 1400 cm⁻¹ is due to antisymmetric and symmetric $\delta(\text{CH}_3)$ modes (peaks at 1480 and 1445 cm⁻¹) [68,74] and may contain a contribution from $\delta(\text{OH})$ deformation mode [67]. The peaks located at 1190 and 1115 cm⁻¹ can be assigned to $\gamma(\text{CH}_3)$ rocking modes [69,70,74], and the peak at 1090 cm⁻¹ to $\nu_{\text{as}}(\text{CO})$ antisymmetric stretching [70,74] of adsorbed methanol and/or methoxy species. The broad band located at ca. 2600 cm⁻¹ can be assigned to a combination band of the methyl rock (1115 cm⁻¹) and methyl deformation (1480 cm⁻¹) modes of adsorbed methoxy species [68,69]. Finally, the broad band centered at ca. 3200 cm⁻¹ can be attributed to the O–H stretching frequency of molecularly adsorbed methanol [67,70].

It should be noted that all vibrational frequencies of adsorbed methanol lie, in general, very close to those of their methoxy counterparts [66–70,72–76] and also to those of adsorbed dimethyl ether [2,70,74]. Thus, it is difficult to determine from the spectra of Fig. 11B the extent to which methanol adsorbs molecularly or in the form of methoxy groups. However, the presence of undissociatively adsorbed methanol is verified by the broad feature located at ca. 3200 cm⁻¹, which is uniquely associated with the O–H stretching frequency of methanol [68–70]. This band is discernible in the spectra recorded in the temperature range of 25–150 °C (traces a–c) and disappears at higher temperatures. This is in agreement with results of TPD experiments of Fig. 12A, which show that weakly held methanol desorbs molecularly from the Al_2O_3 surface in this temperature range.

As shown in the TPD pattern of Fig. 12A, evolution of small amounts of methanol in the gas phase continues at temperatures higher than 150 °C, where molecularly adsorbed methanol is not present on the catalyst surface (Fig. 11B). This indicates that gas-phase methanol may be also formed by combination of surface species according to [65,75]:

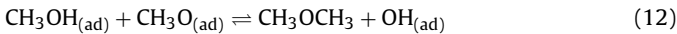


This argument is supported by the observation that heating at 200 °C (Fig. 11B, trace d), which induces desorption of weakly adsorbed methanol, leads in a substantial decrease of the intensity of the negative bands in the $\nu(\text{OH})$ region.

As mentioned above, vibrational frequencies of adsorbed dimethyl ether lie very close to those of adsorbed methoxy species [74]. This may explain the reason why no significant differences are observed in the position of IR bands in the $\nu(\text{C–H})$ region upon heating the sample at 150–250 °C (Fig. 11B, traces c–e), where evolution of DME occurs in the gas phase (Fig. 12A). It may be noted, however, that the pair of peaks at 2938/2822 cm⁻¹ decreases in intensity in this temperature range and that this results in the resolution of the pair of peaks at ca. 2950/2845 cm⁻¹. It may then be suggested that formation of DME involves weakly adsorbed methoxy species (doublet at 2938/2822 cm⁻¹) and not methoxy species that are bonded more strongly on the Al_2O_3 surface (doublet at 2950/2845 cm⁻¹).

Regarding the mechanism of DME formation, it has been proposed that dehydration of methanol over Al_2O_3 catalysts, may occur via two possible routes: The first one involves interaction of adsorbed methoxy species with undissociated methanol (12) [75],

and the second involves reaction between two adsorbed methoxy species adjacent to a hydroxyl group (13) [68,70,77]:



The present results support the second reaction pathway, because DME evolution is observed at temperatures above 150 °C, where only methoxy species, and not molecularly adsorbed methanol, are present on the catalyst surface (Fig. 11B). In addition, evidence is provided that DME production is associated with weakly adsorbed methoxy species.

Increase of temperature above 150 °C results in a progressive decrease of the intensities of all bands associated to methoxy/DME species (Fig. 11B, traces d–i). This is accompanied by the development of new bands located at 2905, 1593, 1395 and 1372 cm⁻¹, which can be attributed to ν(CH), ν_{as}(COO), δ(CH) and ν_s(COO) modes, respectively, of surface formate species [68,70,73,78]. These species may be produced by oxidation of methoxy groups with intermediate formation of dioxomethylene species [65,66,78] or by decomposition of surface methoxy species residing on strong Lewis acid sites [68]. The bands attributed to surface formate species progressively increase in intensity with increasing temperature from 150 to 450 °C (traces c–i) and then disappear upon heating at higher temperatures (spectra not shown for clarity). When methoxy species are completely removed from the catalyst surface, the negative bands in the ν(OH) region return to base line levels, indicating that all O–H bands have been gradually restored to their original shape and intensity.

Comparison of the DRIFT spectra presented in Fig. 11B with the TPD pattern of Fig. 12A shows that conversion of methoxy to

formate species occurs at temperatures where DME production is, practically, diminished and CH₄, H₂ and CO start to evolve in the gas phase. This is in agreement with results of previous studies, which reported that conversion of methoxy into formate species is accompanied by evolution of CH₄ and H₂ [68], whereas decomposition of formates yields CO and H₂O [2]. Careful inspection of the DRIFT spectra of Fig. 11B shows that development of bands attributed to formate species takes place at the expense of those corresponding to the strongly held methoxy species (doublet at 2950/2845 cm⁻¹). Thus, it may be argued that weakly adsorbed methoxy species are converted to DME whereas more strongly held methoxy species are converted to surface formates and, eventually, to CH₄, H₂ and CO in the gas phase.

3.3.3. TPSR of methanol in the absence and in the presence of water

The effects of reaction temperature and feed composition on catalytic activity and selectivity have been investigated with the use of the temperature-programmed surface reaction (TPSR) technique. Results obtained following interaction of the Al₂O₃ catalyst with 0.5%CH₃OH (in He) at 25 °C for 30 min and subsequent linear heating ($\beta = 15^\circ\text{C min}^{-1}$) at 650 °C under the same flow are shown in Fig. 12B, where the MS responses of methanol, DME, CH₄, CO, CO₂ and H₂ are plotted as functions of temperature. It is observed that the TPSR pattern is qualitatively similar to that obtained for TPD of methanol (Fig. 12A). In particular, increase of temperature results in desorption of a substantial amount of weakly adsorbed methanol, which peaks at ca. 90 °C and then decreases abruptly at temperatures higher than ca. 150 °C. This is accompanied by evolution of DME, which is the only reaction product formed in the temperature range of 150–350 °C, in agreement with results of Fig. 8. Further increase of temperature results in the evolution of CH₄, CO and H₂,

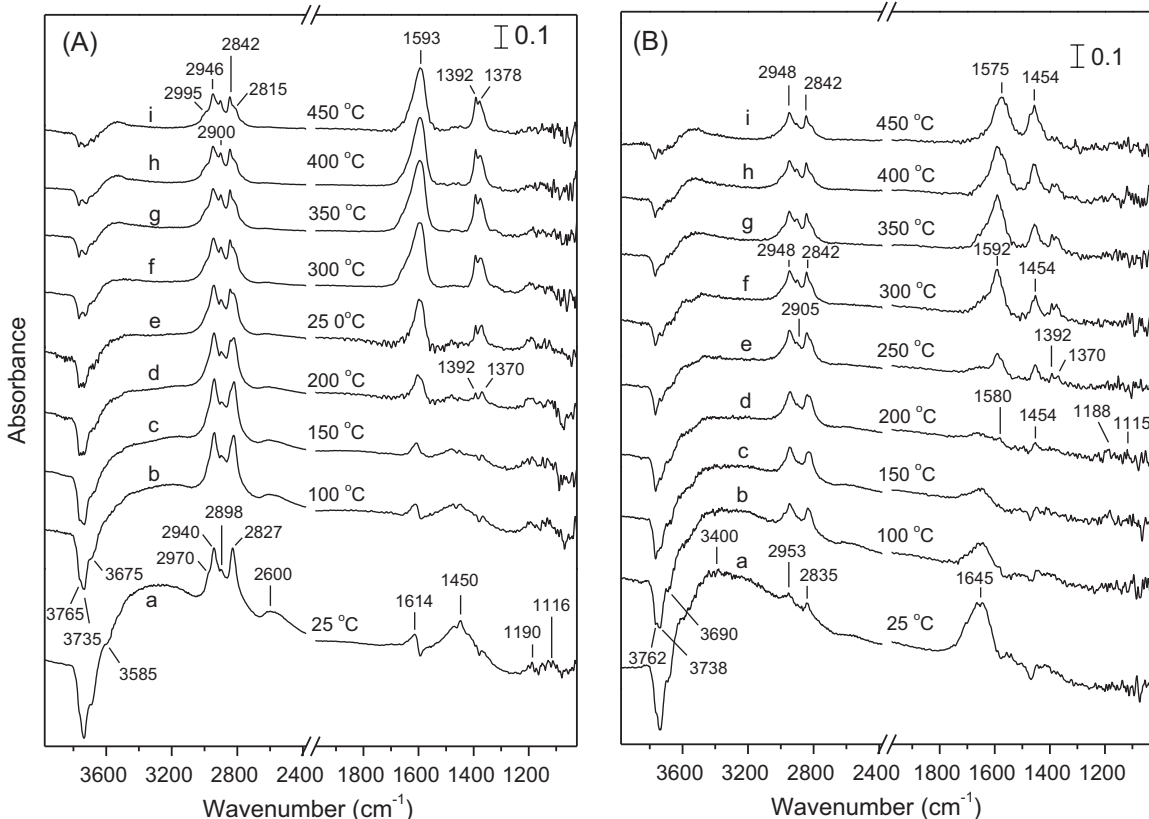


Fig. 13. DRIFT spectra obtained over the Al₂O₃ (Al4) catalyst following interaction with (A) 0.5% CH₃OH (in He) or (B) 0.5% CH₃OH + 1.5% H₂O (in He) at 25 °C for 30 min and subsequent stepwise heating at the indicated temperatures under a flow of the same reaction mixture.

in accordance to the decomposition reactions discussed above. Formation of CO₂ and additional amounts of H₂ at temperatures above 500 °C can be attributed to the occurrence of the WGS reaction (3).

A similar experiment was conducted employing DRIFTS in order to study the nature and population of species present on the catalyst surface under reaction conditions as a function of reaction temperature. Results obtained are summarized in Fig. 13A, which shows spectra recorded following exposure of the catalyst to 0.5% CH₃OH (in He) for 30 min (trace a) and subsequent stepwise heating at 450 °C (traces b–i) under the same reaction mixture. It is observed that spectra obtained in the TPSR experiment of Fig. 13A, i.e., under flowing methanol (in He), are qualitatively similar to those obtained in the TPD experiment of Fig. 11B, i.e., under flowing He. The main difference is that, in the former case (Fig. 13A), absorption peaks attributed to surface formates (located at ca. 2900, 1593, 1392 and 1370 cm⁻¹) appear at lower temperatures, and their relative intensities are much higher, compared to those obtained under He flow (Fig. 11B). Regarding methoxy species, they behave in a way similar to that discussed in Section 3.3.2. In particular, at temperatures up to ca. 150 °C (traces a–c) the surface is populated mainly by the weakly adsorbed methoxy groups characterized by a pair of peaks at 2940/2827 cm⁻¹. At higher temperatures, where production of DME takes place in the gas phase (Fig. 12B), the relative population of this species decreases, providing additional evidence that it is related to DME formation. Finally, at temperatures higher than 400 °C (traces h–i) the catalyst surface is covered mainly by strongly adsorbed methoxy groups (2946/2842 cm⁻¹) and formate species that, as discussed above, are responsible for the evolution of CH₄, H₂ and CO in the gas phase.

The effect of addition of water in the feed has been investigated by DRTIFS-TPSR using a 0.5%CH₃OH + 1.5%H₂O (in He) mixture and spectra obtained are presented in Fig. 13B. It is observed that the spectrum recorded at 25 °C (trace a) is characterized mainly by bands attributed to adsorbed water (compare with Fig. 11A). The appearance of two weak bands at 2953 and 2835 cm⁻¹ indicates that only small amounts of adsorbed methanol/methoxy species are present on the catalyst surface and shows clearly that adsorption of methanol at room temperature is suppressed significantly in the presence of water. Stepwise increase of temperature results in a progressive decrease of the amount of adsorbed water, which diminishes at 200–250 °C (traces d–e), and to a concomitant increase of the coverage of methoxy species, which reaches a maximum in the same temperature range. This is accompanied by the appearance of bands attributed to surface formate species, the intensity of which increases significantly upon further increase of temperature (traces e–i).

It is of interest to note that a couple of new bands located at 1454 and 1575 cm⁻¹ are resolved at 200 °C (trace d) and increase progressively in intensity upon increasing temperature to 450 °C (traces e–i). These bands, which were not observed in TPD (Fig. 11B) and TPSR (Fig. 13A) of methanol, can be attributed to carbonate–carboxylate species [79,80]. These structures are not intermediate compounds in the dehydration of methanol but may be responsible for the occurrence of side reactions that lead to the appearance of H₂ and CO in the gas phase [79].

4. Conclusions

The activity and selectivity of Al₂O₃ catalysts for the dehydration of methanol to dimethyl ether have been investigated over a number of alumina samples of variable physicochemical characteristics. Results show that catalytic behavior is determined by the textural properties, degree of crystallinity and total amount of acid sites of Al₂O₃. As a general trend, catalytic performance is improved significantly with increase of specific surface area, which is evidenced

by a shift of the methanol conversion curve toward lower reaction temperatures. Enhanced catalytic activity of high-SSA samples cannot be attributed solely to the higher amount of surface acid sites (estimated by NH₃-TPD) implying that the reaction rate is determined to a large extent from other parameters, such as textural properties and degree of crystallinity. Conversion of methanol at a given temperature is generally higher for materials with cylindrical pores of an average width of about 9–10 nm, total porosity of 0.60–0.80 cm³ g⁻¹ and crystallite size of ca. 7–9 nm. Materials with higher porosity and/or smaller crystallite size are less active, most probably due to their highly amorphous nature. The apparent activation energy of the reaction is, practically, the same for all studied catalysts taking an average value of 24 ± 4 kcal mol⁻¹. Addition of water vapor in the feed does not influence selectivity to reaction products but results in an increase of the apparent activation energy and in a (reversible) shift of methanol conversion curve toward higher temperatures. Results of mechanistic studies indicate that interaction of methanol with the Al₂O₃ surface results in the formation of two kinds of methoxy groups of different adsorption strength. Evidence is provided that DME evolution is associated with methoxy species that are weakly adsorbed on the Al₂O₃ surface, whereas more strongly held species decompose to yield surface formate and, eventually CH₄ and CO in the gas phase.

Acknowledgement

This research has been co-financed by the European Union (European Social Fund ESF) and Greek national funds through the Operational Program “Education and Lifelong Learning” of the National Strategic Reference Framework (NSRF) – Research Funding Program: Thales. Investing in knowledge society through the European Social Fund (CAT-BIOFUEL project).

Appendix A. Supplementary data

Supplementary data associated with this article can be found, in the online version, at <http://dx.doi.org/10.1016/j.apcatb.2012.11.043>.

References

- [1] T.A. Semelsberger, K.C. Ott, R.L. Borup, H.L. Greene, *Applied Catalysis B* 61 (2005) 281–287.
- [2] E. Ozensoy, D. Herling, J. Szanyi, *Catalysis Today* 136 (2008) 46–54.
- [3] Dimethyl Ether (DME) Technology and Markets, CHEMSYSTEMS PERP Program, PERP07/08-S3, Nexant Inc., <http://www.chemsystems.com/reports/>
- [4] S. Ahlgren, A. Bak, S. Bernesson, A. Nordberg, O. Noren, P.-A. Hansson, *Biosystems Engineering* 99 (2008) 145–155.
- [5] T.A. Semelsberger, R.L. Borup, H.L. Greene, *Journal of Power Sources* 156 (2006) 497–511.
- [6] T.S. Zhao, T. Takemoto, N. Tsubaki, *Catalysis Communications* 7 (2006) 647–650.
- [7] R.B. Diemer, W.L. Luyben, *Industrial and Engineering Chemistry Research* 49 (2010) 12224–12241.
- [8] D. Liu, X. Huang, L. Hu, D. Fang, W. Ying, D. Chen, *Journal of Natural Gas Chemistry* 19 (2010) 165–168.
- [9] J.J. Spivey, *Chemical Engineering Communications* 110 (1991) 123–142.
- [10] C. Arcoumanis, C. Bae, R. Crookes, E. Kinoshita, *Fuel* 87 (2008) 1014–1030.
- [11] Z. Zhu, D.K. Li, J. Liu, Y.J. Wei, S.H. Liu, *Applied Thermal Engineering* 35 (2012) 9–14.
- [12] R. Ladera, E. Finocchio, S. Rojas, J.L.G. Fierro, M. Ojeda, *Catalysis Today* 192 (2012) 136–143.
- [13] D. Cocco, V. Tola, G. Cau, *Energy* 31 (2006) 1446–1458.
- [14] K. Takeishi, H. Suzuki, *Applied Catalysis A* 260 (2004) 111–117.
- [15] T.A. Semelsberger, K.C. Ott, R.L. Borup, H.L. Greene, *Applied Catalysis A-General* 309 (2006) 210–223.
- [16] K. Faungnawakij, T. Fukunaga, R. Kikuchi, K. Eguchi, *Journal of Catalysis* 256 (2008) 37–44.
- [17] T. Fukunaga, N. Ryumon, S. Shimazu, *Applied Catalysis A-General* 348 (2008) 193–200.
- [18] V.M. Mysov, K.G. Ione, *Chemistry for Sustainable Development* 11 (2003) 197–207.
- [19] A.T. Aguayo, J. Erena, I. Sierra, M. Olazar, J. Bilbao, *Catalysis Today* 106 (2005) 265–270.

- [20] G. Centi, S. Perathoner, *Catalysis Today* 148 (2009) 191–205.
- [21] Z. Hosseini, M. Taghizadeh, F. Yaripour, *Journal of Natural Gas Chemistry* 20 (2011) 128–134.
- [22] Q. Tang, H. Xu, Y. Zheng, J. Wang, H. Li, J. Zhang, *Applied Catalysis A-General* 413–414 (2012) 36–42.
- [23] Q. Ge, Y. Huang, F. Qiu, *Reaction Kinetics and Catalysis Letters* 63 (1998) 137–142.
- [24] X.D. Peng, A.W. Wang, B.A. Toseland, P.J.A. Tijm, *Industrial and Engineering Chemistry Research* 38 (1999) 4381–4388.
- [25] S. Lee, A. Sardesai, *Topics in Catalysis* 32 (2005) 197–207.
- [26] G.-X. Qi, J.-H. Fei, X.-M. Zheng, Z.-Y. Hou, *Catalysis Letters* 72 (2001) 121–124.
- [27] J.-L. Tao, K.-W. Jun, K.-W. Lee, *Applied Organometallic Chemistry* 15 (2001) 105–108.
- [28] T. Takeguchi, K.-I. Yanagisawa, T. Inui, M. Inoue, *Applied Catalysis A-General* 192 (2000) 201–209.
- [29] L. Wang, Y. Qi, Y. Wei, D. Fang, S. Meng, Z. Liu, *Catalysis Letters* 106 (2006) 61–66.
- [30] M. Xu, J.H. Lunsford, D.W. Goodman, A. Bhattacharyya, *Applied Catalysis A* 149 (1997) 289–301.
- [31] K.-W. Jun, H.S. Lee, H.-S. Roh, S.-E. Park, *Bulletin of the Korean Chemical Society* 23 (2002) 803–806.
- [32] F. Raoof, M. Taghizadeh, A. Eliassi, F. Yaripour, *Fuel* 87 (2008) 2967–2971.
- [33] A.R. Keshavarz, M. Rezaei, F. Yaripour, *Journal of Natural Gas Chemistry* 20 (2011) 334–338.
- [34] S. Jiang, J.-S. Hwang, T. Jin, T. Cai, W. Cho, Y.S. Baek, S.-E. Park, *Bulletin of the Korean Chemical Society* 25 (2004) 185–189.
- [35] Y. Fu, T. Hong, J. Chen, A. Auroux, J. Shen, *Thermochimica Acta* 434 (2005) 22–26.
- [36] L. Travalloni, A.C.L. Gomes, A.B. Gaspar, M.A.P. da Silva, *Catalysis Today* 133–135 (2008) 406–412.
- [37] V. Vishwanathan, K.-W. Jun, J.-W. Kim, H.-S. Roh, *Applied Catalysis A-General* 276 (2004) 251–255.
- [38] F. Yaripour, F. Baghaei, I. Schmidt, J. Perregaard, *Catalysis Communications* 6 (2005) 542–549.
- [39] M. Mollavali, F. Yaripour, Sh. Mohammadi-Jam, H. Atashi, *Fuel Processing Technology* 90 (2009) 1093–1098.
- [40] V. Vishwanathan, H.-S. Roh, J.-W. Kim, K.-W. Jun, *Catalysis Letters* 96 (2004) 23–28.
- [41] K. Lertjiamrnat, P. Praserthdam, M. Arai, J. Panpranot, *Applied Catalysis A-General* 378 (2010) 119–123.
- [42] M. Mollavali, F. Yaripour, H. Atashi, S. Sahebdelfar, *Industrial and Engineering Chemistry Research* 47 (2008) 3265–3273.
- [43] A.R. Keshavarz, M. Rezaei, F. Yaripour, *Powder Technology* 199 (2010) 176–179.
- [44] G. Leofanti, M. Padovan, G. Tozzola, B. Venturelli, *Catalysis Today* 41 (1998) 207–219.
- [45] F. Dumeignil, K. Sato, M. Imamura, N. Matsubayashi, E. Payen, H. Shimada, *Applied Catalysis A-General* 241 (2003) 319–329.
- [46] J. Aguado, J.M. Escola, M.C. Castro, *Microporous and Mesoporous Materials* 128 (2010) 48–55.
- [47] F. Prinetto, G. Ghiootti, P. Graffin, D. Tichit, *Microporous and Mesoporous Materials* 39 (2000) 229–247.
- [48] D.L. Cocke, E.D. Johnson, R.P. Merrill, *Catalysis Reviews* 26 (1984) 163–231.
- [49] F. Arena, R. Dario, A. Parmaliana, *Applied Catalysis A-General* 170 (1998) 127–137.
- [50] A.T. Shakhtakhtinskaya, Z.M. Mamedova, Sh.F. Mutallibova, S.Z. Alieva, R.G. Mardzhanova, *Reaction Kinetics and Catalysis Letters* 39 (1989) 137–140.
- [51] D.M. Sung, Y.H. Kim, E.D. Park, J.E. Yie, *Research on Chemical Intermediates* 36 (2010) 653–660.
- [52] J. Khom-in, P. Praserthdam, J. Panpranot, O. Mekasuwandumrong, *Catalysis Communications* 9 (2008) 1955–1958.
- [53] A. Corma, V. Fornes, M.I. Juan-Rajadell, J.M. Lopez Nieto, *Applied Catalysis A-General* 116 (1994) 151–163.
- [54] S.M. Kim, Y.-J. Lee, J.W. Bae, H.S. Potdar, K.-W. Jun, *Applied Catalysis A-General* 348 (2008) 113–120.
- [55] E. Kraljeva, R. Palcheva, L. Dimitrov, U. Armbruster, A. Brückner, A. Spojakina, *Journal of Materials Science* 46 (2011) 7160–7168.
- [56] B.T. Diep, M.S. Wainwright, *Journal of Chemical and Engineering Data* 32 (1987) 330–333.
- [57] M. Raimondo, A. De Stefanis, G. Perez, A.A.G. Tomlinson, *Applied Catalysis A-General* 171 (1998) 85–97.
- [58] U.V. Mentzel, K.T. Hojholt, M.S. Holm, R. Fehrman, P. Beato, *Applied Catalysis A-General* 417–418 (2012) 290–297.
- [59] K.C. Tokay, T. Dogua, G. Dogu, *Chemical Engineering Journal* 184 (2012) 278–285.
- [60] J. Toyir, P. Ramirez de la Piscina, J.L.G. Fierro, N. Homs, *Applied Catalysis B* 34 (2001) 255–266.
- [61] L. Vlaev, D. Damyanov, M.M. Mohamed, *Colloids and Surfaces* 36 (1989) 427–437.
- [62] J. Szanyi, J.H. Kwak, R.J. Chimentao, C.H.F. Peden, *Journal of Physical Chemistry C* 111 (2007) 2661–2669.
- [63] H. Knözinger, P. Ratnasamy, *Catalysis Reviews: Science and Engineering* 17 (1978) 31–70.
- [64] S.U. Rege, R.T. Yang, *Chemical Engineering Science* 56 (2001) 3781–3796.
- [65] G. Busca, V. Lorenzelli, *Journal of Catalysis* 66 (1980) 155–161.
- [66] G. Busca, *Catalysis Today* 27 (1996) 457–496.
- [67] G. Busca, P.F. Rossi, V. Lorenzelli, M. Benaisa, J. Travers, J.-C. Lavalle, *Journal of Physical Chemistry* 89 (1985) 5433–5439.
- [68] A.R. McInroy, D.T. Lundie, J.M. Winfield, C.C. Dudman, P. Jones, D. Lennon, *Langmuir* 21 (2005) 11092–11098.
- [69] A.R. McInroy, D.T. Lundie, J.M. Winfield, C.C. Dudman, P. Jones, S.F. Parker, J.W. Taylor, D. Lennon, *Physical Chemistry Chemical Physics* 7 (2005) 3093–3101.
- [70] S. Tamm, H.H. Ingelsten, M. Skoglundh, A.E.C. Palmqvist, *Journal of Catalysis* 276 (2010) 402–411.
- [71] D.T. Lundie, A.R. McInroy, R. Marshall, J.M. Winfield, P. Jones, C.C. Dudman, S.F. Parker, C. Mitchell, D. Lennon, *Journal of Physical Chemistry B* 109 (2005) 11592–11601.
- [72] B.G. Frederick, G. Apai, T.N. Rhodin, *Surface Science* 277 (1992) 337–350.
- [73] S. Bertarione, D. Scarano, A. Zecchina, V. Johaneck, J. Hoffmann, S. Schauermann, J. Libuda, G. Rupprechter, H.-J. Freund, *Journal of Catalysis* 223 (2004) 64–73.
- [74] J.G. Chen, P. Basu, T.H. Ballinger, J.T. Yates Jr., *Langmuir* 5 (1989) 352–356.
- [75] R.S. Schiffino, R.P. Merrill, *Journal of Physical Chemistry* 97 (1993) 6425–6435.
- [76] S. Schauermann, J. Hoffmann, V. Johaneck, J. Hartmann, J. Libuda, *Physical Chemistry Chemical Physics* 4 (2002) 3909–3918.
- [77] V.A. Matyshak, T.I. Kholomenko, G.I. Lin, I.N. Zavalishin, A.Y. Rozovskii, *Kinetics and Catalysis* 40 (1999) 274–295.
- [78] G. Busca, J. Lamotte, J.-C. Lavalle, V. Lorenzelli, *Journal of the American Chemical Society* 109 (1987) 5197–5202.
- [79] L.I. Lafer, V.I. Yakerson, A.M. Rubinshtein, *Russian Chemical Bulletin* 16 (1967) 2312–2318.
- [80] M.C. Sanchez-Sanchez, R.M. Navarro Yerga, D.I. Kondarides, X.E. Verykios, J.L.G. Fierro, *Journal of Physical Chemistry A* 114 (2010) 3873–3882.